Volume 17 Number 33 7 September 2025 Pages 18967-19478

Nanoscale

rsc.li/nanoscale

ISSN 2040-3372



COMMUNICATION

María González-Béjar, Virginie Lhiaubet-Vallet *et al.* Upconversion nanohybrids for NIR-induced photorepair of DNA etheno adducts

Artwork designed by Cora Pardo Asunción.



Nanoscale



COMMUNICATION

View Article Online
View Journal | View Issue



Cite this: Nanoscale, 2025, 17, 19103

Received 30th April 2025, Accepted 28th June 2025 DOI: 10.1039/d5nr01777q

rsc.li/nanoscale

Upconversion nanohybrids for NIR-induced photorepair of DNA etheno adducts†

Laura Francés-Soriano, Da, Gemma M. Rodríguez-Muñiz, Dc
Paloma Lizondo-Aranda, Dc
Delia Bellezza, María González-Béjar * and
Virginie Lhiaubet-Vallet * c

Here, we report NIR-triggered photorepair of DNA damages via photosensitization by using well-known upconversion nanohybrids consisting of ytterbium and erbium co-doped core-shell upconversion nanoparticles (UCs) and Rose Bengal (UC@RB). Specifically, two purine-derived etheno adducts (1, N^6 -etheno-2'-deoxyadenosine (ϵ dA) and 1, N^2 -etheno-2'-deoxyguanosine (ϵ dG)) have been used as proof of concept.

Introduction

Maintaining genome stability is a critical priority for all living organisms. Any change of the original nucleobase sequence can disrupt key biological processes, impair cellular function and potentially induce carcinogenesis or even cell death. Fortunately, mammalian cells have developed multiple and diverse mechanisms to repair the wide range of DNA damage that occurs spontaneously or is induced by exogenous factors. Among them, the discovery of photoreactivation in 1949 was met with significant scientific enthusiasm, marking the inception of the field of DNA repair. Photoreactivation is a unique mechanism that utilizes blue light to reverse *in situ* the UV-induced lesions through the action of photoenzymes called photolyases. It is noteworthy that, up to now, DNA photorepair has been described only for lesions involving pyrimidine dimers. 1

Etheno adducts (ϵ -adducts) are DNA damages present as background lesions in rodent and human tissues. ^{5,6} Initially associated with exposure to human carcinogens such as vinyl chloride, ^{7,8} their presence in unexposed populations has revealed an endogenous origin, primarily through reactions involving metabolically-generated aldehydes derived from lipid peroxidation. ⁹⁻¹¹ Consequently, etheno derivatives represent significant indicators of oxidative stress and have been proposed as potential biomarkers for assessing cancer risk in humans. ^{6,12-15} From a chemical point of view, these lesions contain a five-membered ring formed between an exocyclic amine and a nitrogen atom of the adenine, cytosine or guanine core. Four types of ϵ -adducts have been identified in

[†] Electronic supplementary information (ESI) available: Materials, methods, TEM image, XRD and FTIR spectrum, absorption and emission spectra, kinetic profiles, emission decays fittings, inner filter effect estimation, UCQY, chromatograms, UV and MS spectra of control experiments. See DOI: https://doi.org/10.1039/d5nr01777g

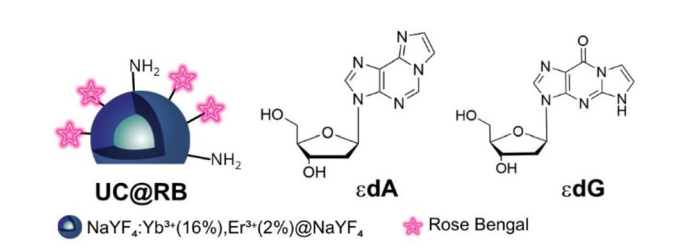


Fig. 1 Representation of the UC@RB nanohybrid and structures of ϵ -adducts.

In recent years, a significant progress has been made in the field of materials science and catalysis, with the aim to emulate the efficiency and selectivity of natural enzymes in synthetic systems. The development of innovative materials that mimic the catalytic behavior of biological enzymes has become a key area of research, aiming to create artificial enzymes, with high and tunable catalytic activity, cost-effectiveness, easy large-scale production, and high stability.^{2–4} In this context, nanomaterials with enzyme-like properties, tagged as "nanozymes", have emerged as alternatives for applications in analytical, environmental, and biomedical applications.^{2–4} Nanozymes are divided into two categories (i) nanomaterials with intrinsic enzyme-like characteristics, and (ii) enzymes or catalytic groups immobilized on nanomaterial surface.⁴

^aInstituto de Ciencia Molecular (ICMol)/Departamento de Química Orgánica, Universitat de València, Calle Catedrático José Beltrán 2, Paterna, Valencia 46980, Spain. E-mail: maria.gonzalez@uv.es

^bDepartamento de Ingeniería Textil y Papelera (DITEXPA), Universitat Politècnica de València, 03801-Alcoy, Spain

^cInstituto Universitario Mixto de Tecnología Química (UPV-CSIC), Universitat Politècnica de València-Consejo Superior de Investigaciones Científicas, 46022-Valencia, Spain. E-mail: lvirgini@itq.upv.es

Communication Nanoscale

DNA: $1,N^6$ -etheno-2'-deoxyadenosine (ε dA, Fig. 1), $3,N^4$ -etheno-2'-deoxycytidine (\(\epsilon\)deoxycytidine (\(\epsilon\)deoxyguanosine (\(\epsilon\)d Fig. 1) and N^2 ,3-etheno-2'-deoxyguanosine (N^2 ,3-edG).

Notably, these ubiquitous lesions are not benign; rather, they exhibit potent mutagenic properties, often leading to base transitions or transversions in mammalian cells. 6,9,16 Their removal is mediated by the well-established base excision repair (BER) initiated by specific DNA glycosylases, ¹⁷ but also by AlkB enzymes, which catalyze a unique oxidative repair of alkylated DNA bases. 18-20

These enzymes are α-ketoglutarate-dependent nonheme iron dioxygenases that utilize α-ketoglutarate and dioxygen on a nonheme iron center to directly reverse the damage to the original nucleobase. 18-20

The photochemical reactivity of ε-adducts has also garnered recent attention. On the one hand, we have recently investigated the photophysics of edC and edG using a combined experimental and theoretical approach, demonstrating that the presence of the etheno ring leads to an increase of the fluorescence quantum yield and a lifetime lengthening. This behavior could be related to a higher photolability of the lesion compared to that of the canonical nucleobase. 21,22

On the other hand, the photoreactivity of the purine derived ε-adducts, εdA and εdG, has been studied in the presence of type I and type II photosensitizers (PSs). 23-25 Interestingly, both ε-adducts were sensitive to photosensitized oxidation by Rose Bengal (RB), yielding photoproducts that correspond to the original nucleosides. Flavin-derived PSs have also been described recently for their potential to repair εdA under blue light irradiation.²⁵ Although the regeneration of the original bases was not complete, these findings point toward photosensitization as a promising new strategy for the photorepair of ε -adducts. ^{23,24}

However, a major limitation of this approach lies in the limited tissue penetration of UV-Vis light, mainly due to absorption by endogenous chromophores such as hemoglobin, melanin, vitamins, flavin cofactors etc.²⁶ To overcome this drawback, near infrared (NIR) light which improves the light penetration depth into tissues due to minimal background absorption, can be used for multiphotonic excitation.²⁷ In this context, ytterbium doped upconversion nanoparticles (UCNPs) loaded or conjugated with PSs can be excited at 980 nm.^{28,29} Moreover, we have recently explored the fundamental mechanism governing the photophysics of the xanthenic dye RB when interacting with core UCNPs (NaYF4:Yb3+, Er³⁺) either anchored to the surface^{30,31} or covalently linked to amino derivatized UCNPs. 32 These upconversion nanohybrids (UCNHs) are capable of generating singlet oxygen (¹O₂) upon excitation with NIR light, transforming lower energy photons into higher-energy photons, which can in turn be absorbed by the PS, i.e. RB, and finally yield ¹O₂ generation. ³⁰⁻³² Both UCNHs were used as photocatalysts for the photooxidation of α -terpinene. 30,31

With this background, we decided to exploit the photosensitizing properties of UCNHs consisting of ytterbium and erbium co-doped core-shell UCNPs (NaYF₄:Yb³⁺(16%),

Er3+(2%)@NaYF4) derivatized with a covalently linked type II photosensitizer (RB), namely UC@RB.

As a proof of concept, this UC@RB was employed as "nanozyme" for NIR-triggered photorepair of the DNA purine-derived etheno adducts.

Results and discussion

Synthesis and characterization of UC@RB nanohybrids

Rose Bengal-capped nanohybrids (UC@RB) were synthesized through a multi-step procedure that includes covalent linkage of RB to the amino derivatized UC surface to avoid leaching during the photorepair process. First, oleate-coated β-NaYF₄: Yb³⁺(16%),Er³⁺(2%) UCNPs were prepared *via* thermal decomposition.33 Then, an inert NaYF4 shell was added by using a layer-by-layer approach, forming core-shell UC@OA nanoparticles.34 TEM images showed hexagonal nanoprisms with a size of $(21.3 \pm 1.4) \times (25.2 \pm 1.4)$ nm (Fig. S1†).

Ligand exchange was then performed using NOBF4 to yield UC@BF4,35 which were subsequently functionalized with 2-aminoethyl dihydrogen phosphate (AEP) to obtain aminofunctionalized UC@AEP NPs.32 The XRD pattern confirmed their β -hexagonal phase structure (Fig. S2 \dagger).

Then, RB hexanoic acid ester (RB-HA) was covalently conjugated to UC@AEP via EDC/NHS-mediated amide coupling, resulting in UC@RB. 32 The successful conjugation of RB to the NP surface was confirmed by infrared (IR) and absorption spectroscopy. The FTIR spectrum clearly shows the characteristic amide bands of UC@RB (Fig. S3†).

Fig. 2 and S4† display the absorbance of the nanohybrids with a broad absorption band in the 500-600 nm range and a shoulder at 520 nm, which is the characteristic absorption spectrum of RB in the UC@RB nanohybrids (RB concentration 5.5×10^{-8} M and 120 RB/UC).³⁰

Fig. 2 also illustrates the upconverted emission spectrum of UC@BF₄, with a significant spectral overlap between the green upconverted emission band of the UCs and the absorption of RB in dimethylformamide (DMF), which is a prerequisite to enable energy transfer (ET) from the UCs to the covalently

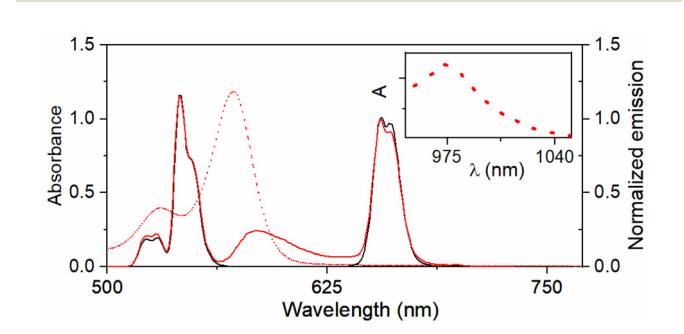


Fig. 2 Absorption spectrum of UC@RB (red dashed line) and normalized UC luminescence spectra ($\lambda_{\rm exc}$ = 980 nm) of UC@BF₄ (black line) and UC@RB (red line) in DMF. Inset: Absorbance in the range 950-1050 nm.

Nanoscale

linked RB upon 980 nm excitation in UC@RB. Considering the inner-filter effect, the corrected upconverted emission spectrum of UC@RB nanohybrids is similar to that of the native UC counterpart (uncorrected spectrum in Fig. S5†). Nonetheless, a new emission band centered around 600 nm is observed and attributed to RB-sensitized luminescence resulting from ET.

To confirm this mechanism, time-resolved photoluminescence measurements were performed at 540 nm, 597 nm, and 650 nm ($\lambda_{\rm exc}$ = 980 nm) (Fig. S6 and Table S1†). The results revealed a clear shortening of the lifetime of the UC green emission due to RB conjugation (93.7 vs. 66.6 µs). More interestingly, the emission band at ca. 600 nm exhibited a notably prolonged lifetime in the µs range (62.5 µs), in contrast to the characteristic ns-scale lifetime for RB (1.3 ns) upon direct excitation in the UC@RB nanohybrid (Fig. S7†). This lifetime lengthening further supports the UC-mediated sensitization of RB and highlights the successful ET process within the UC@RB nanohybrid. Thermally activated delayed fluorescence under N2 and room temperature phosphorescence of ³RB were not detected. Additionally, the presence of the NaYF₄ shell increased ca. 3 times the upconversion quantum yield (UCQY) of the present UC@RB (0.35%) with respect to the analogous Rose Bengal nanohybrid made with core upconversion nanoparticles (0.1%).²⁷

Moreover, the photoactive lanthanides doping the UC can act as acceptors. Accordingly, upon selective excitation of RB in the UC@RB at 572 nm, a clear antenna effect toward the photoactive lanthanide ions in UC@RB was observed as previously observed for analogous nanohybrids made with RB anchored to core UCs.30 As shown in Fig. S8,† two intense near-infrared emission bands emerged, corresponding to the $Yb^{3+} {}^2F_{5/2} \rightarrow {}^2F_{7/2}$ and the $Er^{3+} {}^4I_{11/2} \rightarrow {}^4I_{15/2}$ transitions, respectively. A minor contribution from the ${\rm Er}^{3+}$ $^4{\rm I}_{13/2}
ightarrow$ $^4{\rm I}_{15/2}$ transition cannot be ruled out, although its impact is expected to be limited due to the lower Er3+ content. The emission intensities at both wavelengths were significantly quenched in the presence of oxygen, indicating that under aerobic conditions the observed luminescence arises exclusively from energy transfer involving the singlet excited state of RB (¹RB), as the triplet state (³RB) is effectively deactivated under air. In contrast, under inert atmosphere, both excited states contribute to lanthanide sensitization, with estimated contributions of 60% from ¹RB and 40% from ³RB, respectively.

Oxygen quenching of the RB excited triplet state leads to $^1\mathrm{O}_2$ formation by ET. Consequently, under air direct observation of singlet oxygen phosphorescence at 1270 nm was observed in DMF.‡ The singlet oxygen phosphorescence decay was monoexponential with a lifetime of 17.2 μ s, a reasonable value for DMF as solvent. 36

Evaluation of photorepair activity of UC@RB nanohybrids

The capability of UC@RB nanohybrids to photorepair the ε -adducts upon NIR excitation was assessed. For this purpose, an oxygen-saturated mixture of UC@RB (2 mg mL⁻¹) and the corresponding ε -adduct (10⁻⁴ M) in DMF: H₂O (9:1, v:v) was

irradiated with a 980 nm laser diode. Upon excitation, selective irradiation of the UC moiety within the UC@RB nanohybrid is achieved, enabling UC-mediated sensitization of RB. This process leads to the generation of singlet oxygen, which in turn would promote the intended photorepair.

The ϵ -adducts consumption and photoproducts formation were followed by HPLC coupled to UV-Vis and MS detection. Steady-state photolysis of the ϵ -adducts in the presence of UC@RB nanohybrids led to the appearance of new peaks in the chromatograms (Fig. 3 and 4).

The consumption of the adenine-derived adduct, εdA , led to the formation of a sole photoproduct; thus exhibiting a similar reactivity to that previously reported in literature (Fig. 3). The new peak eluting at t_R 5.3 min was assigned to the canonical nucleoside dA with λ_{max} of 260 nm, a m/z of 252.1, which is identical to that observed for the analysis of an authentic dA sample (Fig. S9†). Indeed, the peak at a retention time (t_R) of 5.9 min detected in the chromatograms with UV and MS detection (Fig. 3A and D) corresponds to that of εdA .

In fact, it exhibits an identical absorption spectrum with a maximum at $\lambda_{\text{max}} = 274$ nm, m/z of 276.1 and t_{R} than an original sample of the lesion (Fig. S10†).

The selected ion monitoring (SIM) traces registered at m/z 252.1 and 276.1 to detect dA and ϵ dA, respectively, agree with these analyses (Fig. 3A, pink and blue lines). In addition, an exact mass m/z 276.1085 ([M + H]⁺: $C_{12}H_{14}N_5O_3$) was found by HRMS analysis for ϵ dA and m/z 252.1088 for dA ([M + H]⁺: $C_{10}H_{14}N_5O_3$, Fig. S11†).

Regarding, the guanine-derived adduct, ϵ dG (eluting at 12.8 min), a more complex chromatogram was observed. Its photodegradation gave rise to the formation of different products with t_R of 4.2, 5.0 and 8.8 min (Fig. 4). Compound eluting at 5.0 min was assigned to the original nucleobase, dG, by comparison with an authentic sample (Fig. S12†). Compounds at t_R 4.2 and 8.8 min, with m/z of 326.1 and 296.1 (Fig. 4), were identified on the basis of our previous study addressing the photosensitization of ϵ dG by RB under visible irradiation. As shown in Fig. S14,† HRMS analyses agree with this assignment, with the detection of m/z 326.1099 (II, $[M+H]^+$: $C_{12}H_{16}N_5O_6$), 268.1034 (dG, $[M+H]^+$: $C_{10}H_{14}N_5O_4$), and 296.0985 (IVa/IVb, $[M+H]^+$: $C_{11}H_{14}N_5O_5$).

Following the mechanism proposed in the literature 23,24 for type II photosensitization of ϵ -adducts (Scheme 1), $^1{\rm O}_2$ addition on the ϵ dG double bond of the etheno ring leads to an elusive dioxetane I (not detected under our experimental conditions) that cleaves to form glycol intermediate II (route A) or intermediate III (route B). Compounds IVa or IVb are obtained from this latter after attack of water, and loss of formic acid. Finally, these intermediates yield the regenerated base dG after a second addition of water and elimination of a second molecule of formic acid. The canonical base dG can also be obtained from intermediate II after attack of water and loss of formic acid dG. A similar mechanism was proposed for dA formation from ϵ dA. 23

Based on this mechanistic scheme, the fast-eluting compound with $t_{\rm R}$ = 4.2 min and m/z of 326.1 corresponds to inter-

Communication

(A) TIC (ESI+) (B) (C) 252.1 SIM m/z 276.1 Intensity $(x 10^{-7})$ ntensity (x10-6) Intensity (x10⁻⁶) SIM m/z 252.1 DMF 8 276.1 0.5 6 8 10 200 350 150 200 250 300 150 250 350 100 100 300 Retention time (min) m/7 m/7 2.0 0.20 (E) (F) (D) Absorbance 0.10 0.05 1.2 0.9 DMF 0.6 0.05 0.3 0.0 0.0

Fig. 3 Analysis of a solution after purification of a mixture of εdA (10⁻⁴ M) and UC@RB in DMF: H₂O (9:1, v:v) irradiated 20 h at 980 nm under O₂ atmosphere. Chromatograms with mass detection (A) TIC (black), SIM at m/z 252.1 (pink) and 276.1 (blue), and corresponding MS spectra of peaks at t_R = 5.3 (B) and t_R = 5.9 min (C). Chromatogram with UV detection at λ = 254 nm (D) and UV-Vis absorption spectra of peaks at t_R = 5.3 (E) and t_R = 5.9 min (F).

300 350 Wavelength (nm)

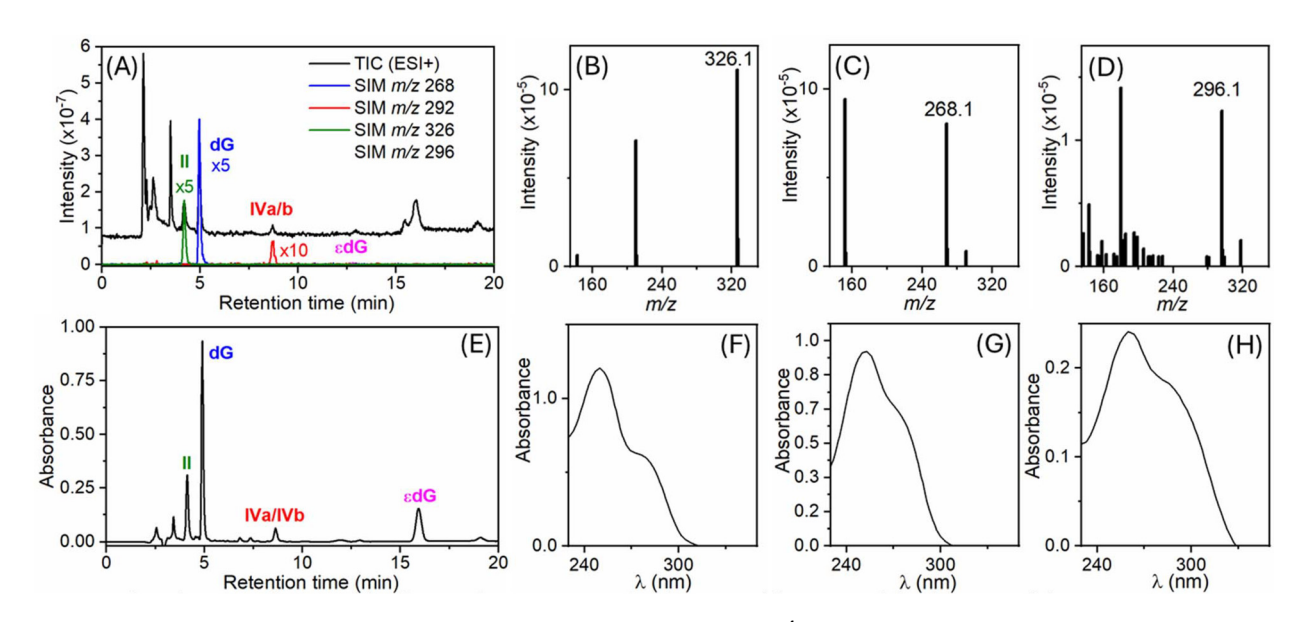


Fig. 4 Chromatograms with mass detection after purification of a mixture of ε dG (10⁻⁴ M) and UC@RB in DMF: H₂O (9:1, v:v) irradiated 5 h at 980 nm under O₂ atmosphere. (A) TIC (black), SIM at m/z 268.1 (blue), 292.1 (pink), 326.1 (green), 296.1 (red), and corresponding MS spectra of peaks at t_R = 4.2 (B), t_R = 5.0 min (C), t_R = 8.8 min (D). Chromatogram with UV detection at λ = 254 nm (E) and UV-Vis absorption spectra of peaks at t_R = 4.2 (F), t_R = 5.0 min (G) and t_R = 8.8 min (H).

mediate II, whereas at $t_R = 8.8$ min the m/z of 296.1 is in line with the generation of intermediate IVa and/or IVb (Scheme 1).

4 6 8 1 Retention time (min)

10

12

250

Control experiments were also performed by irradiating the lesion alone at 980 nm under O_2 conditions. As expected from the lack of ϵ -adducts absorption at this wavelength (Fig. S4†), irradiation of the lesions alone at 980 nm under O_2 conditions does not induce the formation of photoproducts,

confirming their photostability under our experimental conditions (Fig. S15 and S16†). No changes were observed when the lesion is irradiated in the presence of UC@AEP (Fig. S17†). However, dG and intermediates II and IVa/IVb were detected in small amounts under 980 nm irradiation of RB–HA (5.8×10^{-10} M) and the lesions in DMF: H₂O solution (Fig. S18†).

250

400

300

Wavelength (nm)

350

400

Nanoscale Communication

Scheme 1 Proposed mechanism for degradation of ϵ -adducts (here εdG) by a type II process.

Two photon absorption (TPA) has been used as strategy to shift absorption toward the red regions of the spectrum for photodynamic therapy. Therefore, the weak photoreactivity of RB under excitation at 980 nm can be attributed to TPA.²⁷ Comparatively, the irradiation of UC@RB led to higher formation of intermediates II and IV, and of dG (Fig. 4) than for RB-HA (Fig. S18†). This result shows the importance of the FRET process in the excitation of UC@RB and subsequent generation of ¹O₂.

Photoreactivity of RB with canonical nucleosides was also assessed. As expected from a type II PS, only dG suffers degradation (Fig. S19†).

Thus, UC@RB photosensitization of both ε-adducts under O2 conditions restores the original nucleosides, enabling a photorepair mechanism for these lesions.

Based on our previous works^{23,24} and the photophysical results mentioned above a triplet-mediated processes can be proposed, for which upon excitation of the UCNP at 980 nm, resonance ET from the Er³⁺ to RB allows excitation of RB and formation of its triplet excited state. Then, a type II process, involving the formation of ¹O₂ from the triplet excited state of RB should occur as proposed in homogenous solution. ^{23,24}

Methods

Steady-state photolysis

A 200 μ L dispersion containing ϵ dG (1 \times 10⁻⁴ M) or ϵ dA (1 \times 10^{-4} M) and UC@RB (2 mg mL⁻¹) in DMF/H₂O (9:1, v:v) was irradiated at 980 nm with a 5 W continuous wave laser diode (308 W cm⁻²) for 20 or 5 hours under O₂ atmosphere at room temperature. Then, the reaction mixture was purified by centrifugation at 10 000g for 10 min, and the supernatant was filtered and freeze-dried to eliminate DMF and further dissolved in 300 μL of water to be analyzed by HPLC-MS.

Control experiments were carried out under identical conditions (same day, optical setup, laser power and alignment) by irradiating εdG and εdA with NIR light (i) in the absence of UC@RB nanohybrids, and (ii) in the presence of UC@AEP (2 mg mL⁻¹) or (iii) RB-HA (5.8 \times 10⁻¹⁰ M; similar absorbance to that of RB in UC@RB), all in an O₂ saturated atmosphere. Identical purification steps were followed (except centrifugation for RB-HA).

HPLC analyses

Irradiation mixtures were analyzed using an HPLC system composed of Shimadzu modules: a DGU-405 degassing unit, a LC-40D xs solvent delivery module, a SCL-40 system controller, SIL-40C xs autosampler, a CTO-40C column oven, an SPD-M40 Photodiode array detector, and a Triple Quadrupole Mass Spectrometer LC 840 model. A Zorbax Eclipse Plus C18 (100 × 4.6 mm, 3.5 μm) column was used for all the analyses. For εdG photosensitization, the analysis was run under isocratic conditions for 25 min with a mobile phase of 5% acetonitrile and 95% H₂O, both acidified with 0.1% HCOOH, then a gradient was applied to reach 95% of acetonitrile in 10 min, these conditions were maintained for 10 min; the flow rate was set at 0.4 mL min⁻¹. For edA photosensitization, the analysis was run under isocratic conditions for 25 min with a mobile phase of 3% acetonitrile and 97% H₂O, both acidified with 0.1% HCOOH, then a gradient was applied to reach 95% of acetonitrile in 10 min, these conditions were maintained for 10 min; the flow rate was set at 0.5 mL min⁻¹. Analyses were performed using electrospray in positive mode with a capillary voltage of 4.5 kV. The following MS parameters were used: nebulizing gas flow: 3 L min⁻¹, drying gas flow: 15 L min⁻¹, interface temperature: 350 °C, desolvation line temperature: 250 °C, and heating block: 400 °C. The data were processed using Lab Solutions software. The chromatograms were compared with those of pure compounds.

Conclusions

In summary, DNA etheno adducts photorepair has been demonstrated by using a photosensitizer (RB) covalently linked to amino-functionalized ytterbium and erbium codoped core-shell UCs (NaYF4:Yb3+,Er3+@NaYF4), termed UC@RB nanohybrids. These nanohybrids acted as a light-harvesting nanozymes that absorb NIR-light and transfer energy to RB. This sensitization efficiently produced singlet oxygen upon 980 nm excitation as a reactive species for initiating photosensitized oxidative transformations of specific DNA lesions. As proof of concept, two biologically relevant purinederived etheno ε -adducts, 1, N^6 -etheno-2'-deoxyadenosine (ε dA) and $1,N^2$ -etheno-2'-deoxyguanosine (ε dG), have been oxidized in the presence of UC@RB under 980 nm excitation. The photochemical conversion led to the regeneration of their

Communication Nanoscale

respective original nucleosides (dA and dG), most likely through a type II photosensitized mechanism.

Importantly, the use of NIR excitation would allow for deeper and more efficient excitation of ytterbium-doped UCs, enabling photochemical processes in optically challenging environments such as tissues, with reduced scattering and absorption losses. This study illustrates the feasibility of UCNP-based photosensitizer systems for site-specific photochemical DNA repair, with promising implications for non-invasive therapeutic applications.

Future efforts will focus on optimizing synthetic strategies for covalently linked systems to maximize the efficiency of photorepair. Particularly, the preparation of UCNHs with high UCQY through precise structural and compositional engineering, as well, as the exploration of alternative PSs to meet the demanding requirements of light-driven DNA repair strategies.

Author contributions

Laura Francés-Soriano, Gemma M. Rodríguez-Muñiz and Delia Bellezza: investigation, methodology, data curation, visualization, formal analysis, writing – original draft; Paloma Lizondo-Aranda: investigation, methodology, data curation, visualization, formal analysis; María González-Béjar, and Virginie Lhiaubet-Vallet: conceptualization, funding acquisition, project administration, methodology, supervision; writing – review & editing.

Conflicts of interest

There are no conflicts to declare.

Data availability

The data supporting this article have been included as part of the ESI.†

Acknowledgements

Financial support from the Spanish government (projects PID 2021-128348NB-I00 and PID2023-152131NB-I00, Severo Ochoa centre of excellence program CEX 2021-001230-S, Maria de Maeztu excellence program CEX2024-001467-M funded by MICIN/AEI/10.13039/501100011033/ and "FEDER a way of making Europe") are acknowledged. LFS thanks also MCIU, AEI and FSE+, for her Ramón y Cajal contract (RYC2023-043859-I). This study forms part of the Advanced Materials programme (MFA/2022/051) and was supported by MICIN with funding from European Union NextGenerationEU (PRTR-C17. I1) and by Generalitat Valenciana (GVA) (IDIFEDER/2018/064, IDIFEDER/2021/064, CIPROM/2022/57), all of them partially cofinanced with FEDER funds and Conselleria d'Educació, Universitats i Ocupació. We are also grateful for the support

from Horizon Europe Marie Skłodowska Curie Project (No. 101131231). The authors are grateful to SCSIE, University of Valencia for providing TEM and HRMS facilities. The authors gratefully acknowledge Juan Ferrera-González for his assistance during the initial stages of this project. We also thank Julia Pérez Prieto and Miguel A. Miranda for their valuable scientific discussions.

References

 \ddagger Singlet oxygen could not be detected spectroscopically upon 980 nm excitation of UC@RB under our experimental conditions. DMF was used as solvent to get a longer lifetime than in H_2O .

- 1 G. B. Sancar, Mutat. Res., Fundam. Mol. Mech. Mutagen., 2000, 451, 25–37.
- 2 Y. Huang, J. Ren and X. Qu, Chem. Rev., 2019, 119, 4357–4412.
- 3 M. Liang and X. Yan, Acc. Chem. Res., 2019, 52, 2190-2200.
- 4 M. Zandieh and J. Liu, Adv. Mater., 2024, 36, 2211041.
- 5 F. L. Chung, H. J. C. Chen and R. G. Nath, *Carcinogenesis*, 1996, 17, 2105–2111.
- 6 Y. Yu, Y. Cui, L. J. Niedernhofer and Y. Wang, *Chem. Res. Toxicol.*, 2016, **29**, 2008–2039.
- 7 A. K. Basu, M. L. Wood, L. J. Niedernhofer, L. A. Ramos and J. M. Essigmann, *Biochemistry*, 1993, 32, 12793–12801.
- 8 A. Barbin, H. Bartsch, P. Leconte and M. Radman, *Nucleic Acids Res.*, 1981, 9, 375–387.
- 9 B. Tudek, D. Zdżalik-Bielecka, A. Tudek, K. Kosicki, A. Fabisiewicz and E. Speina, *Free Radical Biol. Med.*, 2017, 107, 77–89.
- 10 F. El Ghissassi, A. Barbin, J. Nair and H. Bartsch, *Chem. Res. Toxicol.*, 1995, **8**, 278–283.
- 11 A. Barbin, H. Ohgaki, J. Nakamura, M. Kurrer, P. Kleihues and J. A. Swenberg, *Cancer Epidemiol. Biomarkers Prev.*, 2003, 12, 1241–1247.
- 12 S. S. Hecht, Chem. Res. Toxicol., 2017, 30, 367-375.
- 13 T. Obtułowicz, A. Winczura, E. Speina, M. Swoboda, J. Janik, B. Janowska, J. M. Cieśla, P. Kowalczyk, A. Jawien, D. Gackowski, Z. Banaszkiewicz, I. Krasnodebski, A. Chaber, R. Olinski, J. Nair, H. Bartsch, T. Douki, J. Cadet and B. Tudek, *Free Radical Biol. Med.*, 2010, 49, 1064–1071.
- 14 C. C. M. Garcia, F. P. Freitas, P. Di Mascio and M. H. G. Medeiros, *Chem. Res. Toxicol.*, 2010, 23, 1245– 1255.
- 15 H. Chen, S. Krishnamachari, J. Guo, L. Yao, P. Murugan, C. J. Weight and R. J. Turesky, *Chem. Res. Toxicol.*, 2019, 32, 1850–1862.
- 16 S. Akasaka and F. P. Guengerich, *Chem. Res. Toxicol.*, 1999, 12, 501–507.
- 17 L. Gros, A. A. Ishchenko and M. Saparbaev, *Mutat. Res., Fundam. Mol. Mech. Mutagen.*, 2003, 531, 219–229.
- 18 C. Yi, G. Jia, G. Hou, Q. Dai, W. Zhang, G. Zheng, X. Jian, C.-G. Yang, Q. Cui and C. He, *Nature*, 2010, **468**, 330–333.
- 19 Y. Mishina, C.-G. Yang and C. He, *J. Am. Chem. Soc.*, 2005, **127**, 14594–14595.

Nanoscale

20 D. Zdżalik, A. Domańska, P. Prorok, K. Kosicki, E. van den Born, P. Ø. Falnes, C. J. Rizzo, F. P. Guengerich and B. Tudek, DNA Repair, 2015, 30, 1-10.

- 21 P. Lizondo-Aranda, T. Gustavsson, L. Martínez-Fernández, R. Improta and V. Lhiaubet-Vallet, Chem. - Eur. J., 2024, 30, e202401835.
- 22 P. Lizondo-Aranda, L. Martínez-Fernández, M. A. Miranda, R. Improta, T. Gustavsson and V. Lhiaubet-Vallet, J. Phys. Chem. Lett., 2022, 13, 251-257.
- 23 P. Lizondo-Aranda, G. M. Rodríguez-Muñiz, M. A. Miranda, B. Heyne and V. Lhiaubet-Vallet, Photochem. Photobiol. Sci., 2025, 24, 1-12.
- 24 G. R. Martinez, H. Brum, G. L. Sassaki, L. M. de Souza, A. P. M. de Loureiro, M. H. G. de Medeiros and P. Di Mascio, Biol. Chem., 2018, 399, 859-867.
- 25 Y. M. He, A. Burkard, C. S. Wu, X. Y. Jin, L. Liu, M. Helm and L. Cheng, Angew. Chem., Int. Ed., 2025, 64, e202415417.
- 26 J. M. Dąbrowski and L. G. Arnaut, Photochem. Photobiol. Sci., 2015, 14, 1765-1780.
- 27 S. Brown, Nat. Photonics, 2008, 2, 394-395.
- 28 P. Zhang, W. Steelant, M. Kumar and M. Scholfield, J. Am. Chem. Soc., 2007, 129, 4526-4527.

- 29 A. Nsubuga, K. Morice, N. Fayad, F. Pini, V. Josserand, X. Le Guével, A. Alhabi, M. Henry, D. Puchán Sánchez, N. Plassais, P. Josse, J. Boixel, P. Blanchard, C. Cabanetos and N. Hildebrandt, Adv. Funct. Mater., 2025, 35, 2410077.
- 30 L. Francés-Soriano, D. Bellezza, J. Ferrera-González, M. González-Béjar and J. Pérez-Prieto, Nanoscale Adv., 2024, 6, 5889-5896.
- 31 J. Ferrera-González, M. González-Béjar and J. Pérez-Prieto, Nanoscale, 2023, 15, 19792-19800.
- 32 K. Liu, X. Liu, Q. Zeng, Y. Zhang, L. Tu, T. Liu, X. Kong, Y. Wang, F. Cao, S. A. G. Lambrechts, M. C. G. Aalders and H. Zhang, ACS Nano, 2012, 6, 4054-4062.
- 33 S. Wilhelm, M. Kaiser, C. Würth, J. Heiland, C. Carrillo-Carrion, V. Muhr, O. S. Wolfbeis, W. J. Parak, U. Resch-Genger and T. Hirsch, Nanoscale, 2015, 7, 1403-1410.
- 34 X. Li, D. Shen, J. Yang, C. Yao, R. Che, F. Zhang and D. Zhao, Chem. Mater., 2013, 25, 106-112.
- 35 A. Dong, X. Ye, J. Chen, Y. Kang, T. Gordon, J. M. Kikkawa and C. B. Murray, J. Am. Chem. Soc., 2010, 133, 998-1006.
- 36 S. Oelckers, T. Hanke and B. Röder, J. Photochem. Photobiol., A, 2000, 132, 29-32.